INVITED PAPER

Parametric Nonlinear Silicon-Based Photonics

This paper discusses nonlinear optics in silicon photonics. Because of the tight optical confinement, very compact nonlinear devices can be made in silicon photonics. Applications include the generation of octave-spanning optical frequency combs for making precise clocks.

KANGMEI LI, *Student Member IEEE*, AND AMY C. FOSTER, *Member IEEE*

ABSTRACT | Integrated silicon photonics is revolutionizing the field of optical communications as hybrid photonic/electronic integrated circuits made from this semiconductor material can seamlessly process signals spanning both the optical and electrical domains. The enormous bandwidth afforded by optical signaling enables extremely high aggregate data-rate communication signals. Correspondingly, signal processing devices must employ new mechanisms to keep up with the ever increasing need for greater capacity in communications. To this end, parametric nonlinear optical interactions in silicon-based materials provide a route toward processing and handling signal bandwidths well beyond a THz. These integrated silicon-based photonic structures also benefit from high optical confinement, large nonlinear optical responses, and long interaction lengths, making them highly suitable for power-efficient parametric nonlinear optical interactions. In particular, the parametric nonlinear optical interaction of four-wave mixing (FWM) in silicon-based photonic devices has enabled a wealth of devices for next-generation information handling applications including communications, all-optical computing, metrology, and security, which will be highlighted in this review.

KEYWORDS | Four-wave mixing; nonlinear optical devices; photonic integrated circuits; silicon photonics

I. INTRODUCTION

Light-matter interactions already have a strong foothold in technologies that shape our daily lives from the high-bandwidth long-haul communications links powering our internet backbone to laser machining in manufacturing and medical imaging/diagnostics [1]. In the communications domain, the low cost and high performance of traditional linear silicon photonic devices is becoming indispensable to address the communication volumes demanded by today's short distance communications links. Beyond linear optics, a great deal of research over the past two decades has focused on exploiting the unique technologies developed for silicon photonics for nonlinear optical interactions [2]–[4]. The high lateral optical confinement as well as the ability to propagate over relatively long interaction lengths makes silicon-based integrated photonics very desirable for nonlinear optical devices. By leveraging the efficiency and speed of all-optical processing, the field of nonlinear silicon photonics promises to have a substantial impact in many areas of information technology ranging from traditional telecommunications to some more recently explored areas such as spectroscopy, optical frequency metrology, and information security.

II. PARAMETRIC NONLINEAR SILICON PHOTONICS

Nonlinear-optical effects in silicon-based photonics span a broad range of interactions that can be described as either parametric (essentially instantaneous where energy remains in the form of photons) or nonparametric (energy is transferred to other forms such as heat and sound and the interaction is noninstantaneous). This paper will focus on the parametric nonlinear optical processes due to their speed and versatility of applications.

Parametric nonlinear silicon photonics exploits the ultrafast bound electronic response of silicon-based materials. The parametric nonlinearities of a material arise from higher order terms of the Taylor expansion of the dielectric

Manuscript received February 25, 2018; revised September 27, 2018; accepted October 7, 2018. Date of publication November 8, 2018; date of current version November 20, 2018. This work was supported by the National Science Foundation (NSF) Emerging Frontiers & Multidisciplinary Activities (EFMA) under Grant EFRI ACQUIRE #1641094 and Grant (NSF) ECCS #1521424. *(Corresponding author: Amy C. Foster.)*

The authors are with Johns Hopkins University, Baltimore, MD 21218 USA (e-mail: kli21@jhu.edu; amy.foster@jhu.edu).

Digital Object Identifier 10.1109/JPROC.2018.2876515

polarization field

$$P(t) = \varepsilon_0(\chi^{(1)}E(t) + \chi^{(2)}E^2(t) + \chi^{(3)}E^3(t) + \cdots) \quad (1)$$

where $\chi^{(1)}$ represents the linear term, $\chi^{(2)}$ is the second-order nonlinearity, and $\chi^{(3)}$ is the third-order nonlinearity. As is typical for such expansions, the coefficients for each higher order term are many orders of magnitude smaller than the proceeding term. Thus, a higher electric field amplitude $E(t)$ is required to provide significant contributions from higher order terms to the overall polarization field. In centrosymmetric materials (such as typical silicon-based materials), the second-order term $\chi^{(2)}$ disappears and nonlinear interactions require use of the third-order term (Kerr effect). As one illustrative example, from this term we can obtain the nonlinear refractive index (Kerr coefficient) n_2 which gives rise to an intensity-dependent refractive index of the material: $n_{\text{tot}} = n_{\text{lin}} + n_2 I$, where n_{lin} represents the linear refractive index and I corresponds to the intensity of the light in the material. When comparing n_2 of various silicon-based materials as shown in Table 1, we see that the contribution to the total refractive index from n_2 itself (given, for example, an intensity of $\sim$1 W/cm^2) is many orders of magnitude lower than the linear refractive index. However, in silicon-based waveguide platforms, the tight confinement of light in the high refractive index contrast device enables very high intensities of light with modest optical powers. Therefore, the intensity-dependent refractive index in such platforms can be significant and exploited for nonlinear optical interactions. For example, for a modest optical power of about tens of milliwatts in a waveguide with tight confinement, the intensity can be considerable ($> 10^8$ W/cm^2), thereby producing a significant optically induced modification to the refractive index.

A. Optical Properties of Silicon-Based Platforms

Silicon-based photonic technologies generally make use of planar fabrication of optical waveguiding structures. A dielectric optical waveguide is a device that can confine and propagate light through total internal reflection as a result of its regions of differing refractive index. Generally, this is achieved with an increased refractive index (core) surrounded by a lower refractive index medium (cladding) [5], [6]. The size of mode area depends on the waveguide geometry and the refractive index contrast between the core and cladding material, where a higher refractive index contrast can result in higher confinement of light. Another way to guide light is through interference effects produced by periodic refractive index changes, such as photonic crystal structures, where waveguides are formed by introducing line defects in photonic crystal lattices [7], [8].

Crystalline silicon (c-Si), typically in the form of silicon-on-insulator (SOI), has been used for integrated electronic circuits for decades, and is therefore a natural choice for integrated photonics. Crystalline silicon has a high linear refractive index of 3.48 at telecom wavelengths (near 1550 nm). The high refractive index contrast between c-Si and the cladding material (usually silicon dioxide, which has a linear index around 1.45 at 1550 nm) allows strong light confinement in submicrometer scale c-Si waveguides (hundreds of nanometers in both width and thickness), and hence can provide very high optical intensities with moderate optical powers; a critical parameter for nonlinear optical interactions. In addition, the nonlinear refractive index of c-Si [5], [6] is two orders of magnitude larger than silica fiber. Due to these merits, a significant amount of research has explored the potential use of c-Si devices for nonlinear optical applications. However, the nonlinear loss of c-Si due to two photon absorption (2PA) and free carrier absorption (FCA) is also relatively high, which can impair the nonlinear performance of integrated c-Si devices.

Besides c-Si, other silicon-based materials, each with its own merits, have drawn considerable attention. Silicon nitride (SiN_x) [3], [9] and closely related high-index doped silica (Hydex) [3], [10], [11], while possessing nonlinear refractive indices that are one order of magnitude smaller than c-Si, exhibit much lower linear and nonlinear loss compared to c-Si, and hence can enable resonators with extremely high-quality factors, showing outstanding performance as nonlinear optical sources in spectroscopy and optical frequency metrology applications, as will be discussed in Section IV. Hydrogenated amorphous silicon (a-Si:H) [12]–[17], originally used for solar cells, has recently been explored for nonlinear optical applications. Despite the large variation of a-Si:H properties (depending on deposition parameters), the material generally shows remarkably high nonlinear refractive index (one order of magnitude higher than c-Si) and a linear refractive index comparable to c-Si, which allows ultralow power nonlinear interactions. Furthermore, the effect of nonlinear loss in a-Si:H can be smaller than c-Si, showing a higher nonlinear figure of merit (FOM). One challenge of a-Si:H devices is the light-induced degradation (often attributed to the Staebler–Wronski effect) [18], [19], in which the properties of a-Si:H devices sometimes degrade over time at high optical intensities. This effect is not yet well understood and does not impact all a-Si:H devices, but it is presumably associated with dangling bond defects [19]. Nevertheless, it has been shown experimentally that in some cases the degradation can be reversed through annealing [12]. The properties of waveguides using Si-based materials are summarized in Table 1; the properties of single-mode fiber (SMF) [20] and highly nonlinear fiber (HNLF) [21] are also listed here for comparison. Notably, all of these silicon-based materials are compatible with the complimentary metal–oxide–semiconductor (CMOS) fabrication technology pervasive in semiconductor electronics.

B. Nonlinear Phase Shift

An informative way to quantify a waveguide's nonlinearity is to consider the nonlinear phase shift that is induced

Table 1 Typical Optical Properties of Different Si-Based Waveguides and Fibers at 1550 nm

properties	SMF [20]	HNLF [21]	Hydex Waveguide [3,10,11]	typical SiNx waveguide [3,9]	typical c-Si waveguide [5,6]	typical a-Si:H waveguide [12-16]
mode profile	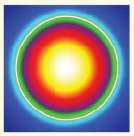		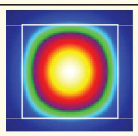 5X enlarged	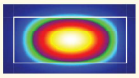 5X enlarged	 5X enlarged	 5X enlarged
effective area (μm^2)	85	12	2	1	0.1	0.1
core index	1.47	1.48	1.7	2	3.48	3.4-3.7
effective index (n_{eff})	1.47	1.46	1.6	1.8	2.3	2.3
n_2 (cm^2/W)	~2 x 10^{-16}	~3 x 10^{-16}	1.15 x 10^{-15}	2.5 x 10^{-15}	4.3 - 6 x 10^{-14}	2.1 - 7.4 x 10^{-13}
γ ($W^{-1}m^{-1}$)	~0.001	0.011	0.23	1	350 - 500	770 - 3000
linear loss (dB/cm)	1.8 x 10^{-6}	9 x 10^{-6}	<0.1	< 0.1	3	5
β_{2PA} (cm/GW)	0	0	0	0	0.45 - 0.87	0.25 - 7
FOM_{2PA}	>>1	>>1	>>1	>>1	0.32 - 0.86	0.46 - 5

Note: In the mode profile plots, the integrated waveguides are enlarged by 5 times in both width and thickness.

with a given optical input power. The nonlinear phase shift due to the intensity-dependent refractive index is

$$\varphi_{\mathrm{NL}} = \gamma P_p L_{\mathrm{eff}} \tag{2}$$

where the effective nonlinearity γ is dependent on the nonlinear refractive index n_2, the effective mode area A_{eff}, and the free-space wavelength

$$\gamma = 2\pi n_2/(\lambda A_{\mathrm{eff}}). \tag{3}$$

The other terms in the equation are P_p, peak pump power (intensity ~ power/area), and L_{eff}, effective length, including loss, over which the nonlinear interaction occurs. If a continuous wave laser is used, then peak pump power P_p is the same as the average pump power; while in the case of a pulsed laser, the effective pump power within the pulse duration is approximately the peak pump power, which can be several orders of magnitude higher than the average power. Thus, pulsed operation can produce high nonlinear efficiency while maintaining a low average pump power. Compared to a bulk medium, a waveguiding structure can greatly increase the interaction length over which the nonlinear phase can accumulate. Furthermore, utilizing silicon-based materials with larger (linear) refractive indices as the waveguide core material can provide a small effective area of $\sim 0.1\ \mu m^2$, which can, for example, be about 750 times smaller compared to the effective area of a standard SMF ($75\ \mu m^2$). In addition, n_2 of silicon-based materials can be about three orders of magnitude larger (e.g., n_2 of a-Si:H is around 5×10^{-13} cm^2/W, while n_2 of fiber is around 2×10^{-16} cm^2/W (see Table 1); however, the linear loss of such waveguides is also six orders of magnitude higher.

Thus, to compare the overall nonlinearity of optical waveguides and fibers, we must consider the effective length, which takes into account the linear propagation loss. Effective length refers to the length of a waveguide considering the loss mechanisms. Here we incorporate linear loss (α) mechanisms into the effective length and use the equation

$$L_{\mathrm{eff}} = (1 - \exp(-\alpha L))/\alpha. \tag{4}$$

To emphasize the benefits of integrating waveguides in a silicon platform for nonlinear optical interactions, the nonlinear phase shift per watt of optical input power (ignoring nonlinear-loss mechanisms) is plotted as a function of length for a variety of silicon-based integrated platforms, as well as fibers in Fig 1. As shown on this log–log plot, all waveguide platforms have a length at which the total nonlinear phase shift will saturate and, if one was only concerned with phase shift with a given power, the larger propagation loss of integrated waveguides would not offset the benefits of the higher nonlinearity and greater mode confinement. However, the most striking trend indicates that higher confinement, higher nonlinearity platforms, such as crystalline silicon (c-Si) and hydrogenated amorphous silicon (a-Si:H), benefit from significantly higher nonlinear phase shifts at short length scales. For example, at a given power (and assuming no nonlinear loss), a 1-cm-length a-Si:H waveguide undergoes 10^5 times more nonlinear phase shift than the same length of HNLF. Thus, it is evident that such higher confinement platforms enable much shorter and more compact nonlinear optical devices with

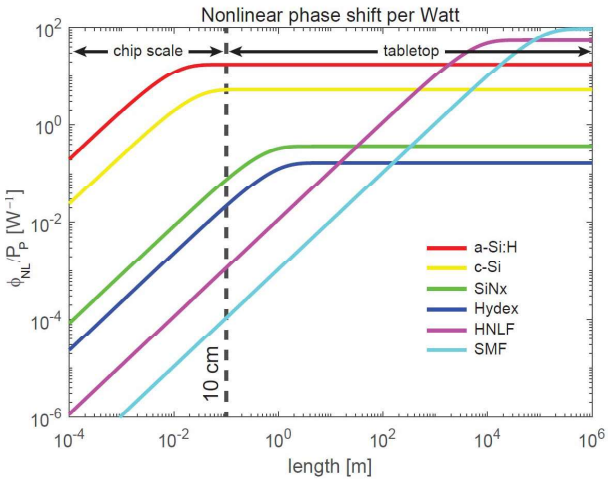

Fig. 1. *Nonlinear phase shift per watt as a function of length for a variety of silicon-based integrated platforms and fibers (ignoring nonlinear loss mechanisms).*

a corresponding ability to scale up the number of devices operating in a system. Such a reduction in device length is also particularly important for parametric processes where the operating bandwidth of the nonlinear interaction is inversely proportional to length [22], and in applications where the addition of significant latency is undesirable (the latency for a given nonlinear phase shift/watt can vary over ~6 orders of magnitude depending on a choice of a-Si:H over SMF, as shown in Fig. 1).

Nonlinear loss mechanisms will limit the performance of a nonlinear optical interaction. Each platform experiences its own set of nonlinear loss mechanisms that vary with each demonstration due to differing material deposition and fabrication conditions as well as device geometries, and due to the specific operating conditions including wavelength, pulse duration, and repetition rate. As such, their effects are excluded from Fig. 1. The general trend in the platforms discussed here is that higher confinement platforms suffer from more significant nonlinear losses. However, at low optical powers, the approximate depiction of nonlinear phase shift as a function of length as shown in Fig. 1 is accurate, and the notable trends aforementioned remain valid. A discussion of the nonlinear loss mechanisms is included in Section II-D and is analyzed for a few platforms in [23].

C. Dispersion

The dispersion of a waveguiding device is critically important to the performance of parametric nonlinear optical processes. Dispersion arises from the dependence of the phase velocity v_p of a lightwave on its frequency ω, and can result, for example, in temporal broadening of an optical pulse as it propagates along the waveguide. The ability to control the dispersion of the waveguide is essential in nonlinear optical processes in which several lightwaves of differing frequencies are involved. Efficient interactions usually require that the sum of wavevectors $k = \omega/v_p$ of the input waves equals the sum of wavevectors of the generated waves, which is termed the phase-matching condition and can be achieved by designing the dispersion of the device [24]. For example, slightly anomalous group-velocity dispersion is generally desired for efficient four-wave mixing (FWM), as will be discussed in details in Section IV.

Here we introduce the group velocity dispersion parameter β_2 (defined as $\beta_2 = \partial^2 k/\partial\omega^2$) and D (defined as $D = -\beta_2 \cdot 2\pi c/\lambda^2$, where c is the speed of light, and λ is the wavelength); $D < 0$ is termed normal dispersion, and $D > 0$ is termed anomalous dispersion. Bulk silicon-based materials typically exhibit large normal dispersion at telecommunication wavelengths, which is generally not ideal. Fortunately, strong optical mode confinement in waveguides can help counteract the material dispersion and obtain anomalous group-velocity dispersion (GVD). A great deal of work has been performed to investigate GVD engineering of waveguides [5], [22], [25]–[28]. Generally, GVD can be tuned through choice of waveguide cross-sectional dimensions; as an example, Fig. 2 depicts how the GVD of a-Si:H waveguides changes with the width and thickness.

The technique of tailoring the waveguide dispersion has enabled a wide range of highly efficient parametric nonlinear optical processes, including wavelength conversion [14], [22], [26], [28], parametric amplification [5], [28], [29], soliton generation [27], supercontinuum generation [30]–[32], and frequency combs [9], [11], [33] in submicrometer waveguides and resonators. In addition, techniques like quasi-phase matching have been explored to further enhance the efficiency and extend the operational bandwidth of the nonlinear processes [34]–[36].

D. Nonlinear Loss

An additional consideration for parametric processes in silicon-based photonic devices is loss arising from the presence of large optical intensities. Typically, a photon at telecommunications wavelength (around 1550 nm) cannot be absorbed directly by silicon-based materials; crystalline silicon, for example, has a bandgap of 1.1 eV, which is higher than the photon energy at 1550 nm (corresponding to 0.8 eV). However, multiple photons in combination can exceed the bandgap energy and be absorbed simultaneously, resulting in loss of photons. These multiphoton

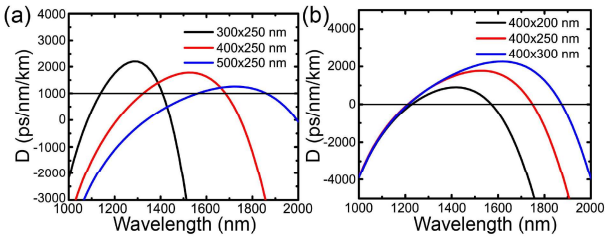

Fig. 2. *Dispersion of a-Si:H waveguides (a) with varying widths and (b) with varying thicknesses.*

absorption processes, such as two photon absorption (2PA) and three photon absorption (3PA), can cause significant loss when operating with high optical intensities. Characterization of the nonlinear optical performance of a material can be quantified to some degree using the nonlinear FOM, which is typically defined as (considering 2PA only)

$$\mathrm{FOM}_{2\mathrm{PA}} = \frac{n_2}{\beta_{2\mathrm{PA}} \cdot \lambda} \tag{5}$$

where $\beta_{2\mathrm{PA}}$ is the 2PA coefficient and λ is the wavelength.

In addition to the absorption of multiple photons directly, carriers (electrons and holes) are generated as a byproduct in multiphoton absorption processes. The generated carriers can then be excited to a higher energy state by consuming other photons through single-photon absorption, leading to additional loss; this process is named free carrier absorption (FCA). Besides absorption, free carriers also limit the operational speed of optical devices due to their long lifetime (on the order of nanoseconds) [37]. Additionally, defects such as surface states and material defects (for example, dangling bonds in a-Si:H) create mid-gap localized states, which aid sequential one-photon absorption by the so-called two-state absorption (TSA) process [38]–[40]. The presence of free carriers also results in a refractive index change and resulting phase shift, which is termed free carrier dispersion (FCD). The phase shift induced by FCD opposes that induced by the Kerr effect, thus the total achievable nonlinear phase shift is reduced [41]. The nonlinear losses due to multiphoton, defect state, and FCA as well as FCD hamper nonlinear processes and limit the maximum achievable efficiency [26], [41]–[44].

A variety of techniques have been developed to alleviate the effects of nonlinear loss. Generally, multiphoton absorption cannot be easily reduced in crystalline materials, which have a fixed band structure; on the contrary, band structures can be tuned in noncrystalline materials like a-Si:H [45], providing an opportunity to increase the bandgap energy and hence reduce multiphoton absorption [42]. Furthermore, structures such as reverse-biased p–i–n junctions [37], [46] and metal–semiconductor–metal junctions [47], [48] have been utilized to remove generated free carriers, and experimental demonstrations show great reduction of the free-carrier lifetime (from 3 ns to 12.2 ps), improved conversion efficiency in nonlinear processes [49]–[51], and increased operational speed [52] due to rapid free carrier removal. To reduce surface defects, a thin layer of dielectric films (such as aluminum oxide) can be grown on the top to passivate the surface of c-Si devices [53]–[55]. To reduce the material defect states in a-Si:H, deposition parameters must be carefully chosen to facilitate the formation of Si-H bonds, which helps reduce the defects arising from dangling bonds [42], [56], [57].

III. SELF-PHASE AND CROSS-PHASE MODULATION

When a high-intensity pulse (intensity is varying in time) propagates through a nonlinear medium, it experiences a time-dependent phase shift with the same temporal shape as the pulse intensity due to the intensity-dependent nonlinear refractive index $\Delta n(t) = n_2 I(t)$. This effect is known as self-phase modulation (SPM). As a consequence of this time-dependent phase shift, the pulse typically broadens in the spectral domain. In one respect, SPM presents an efficient way to characterize the nonlinear refractive index n_2 of materials, as studied in [40], [58]. In the extreme case, SPM can be employed to achieve supercontinuum generation (an extremely wide spectral spanning light source). Reports have shown wide spectral-spanning supercontinuum generation in c-Si [30], [59]–[62], SiN_x [63]–[67], and a-Si:H waveguides [31], [32], [68]. As one example, 550-nm spectral broadening at telecommunication wavelengths is obtained in a-Si:H waveguides of different widths [32]; output spectra with varying peak powers in one sample waveguide are shown in Fig. 3, denoting the various mechanisms contributing to supercontinuum generation. Such broadband supercontinuum sources have applications in optical frequency metrology, optical coherence tomography, and wavelength division multiplexing.

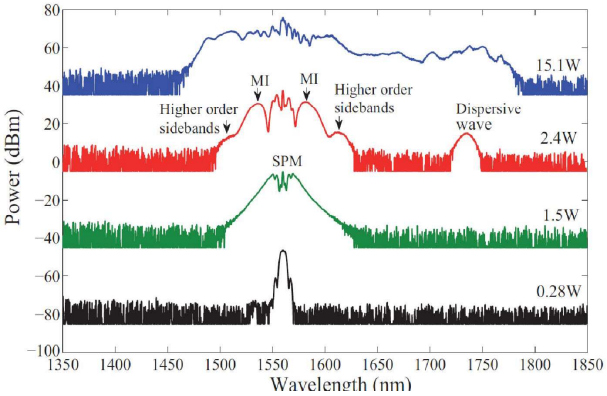

Fig. 3. *Supercontinuum generation in an a-Si:H waveguide: output spectra with varying on-chip peak pump powers. Figure reproduced with permission from [32], ©2014 OSA.*

When two or more optical waves with different wavelengths are launched simultaneously into a waveguide, they can interact through cross-phase modulation (XPM), in which one optical wave induces a phase shift on another wave. Such phase shift induced by XPM can find a range of applications such as spectral broadening [69], optical switching [70], [56], and signal regeneration [71].

IV. FOUR-WAVE MIXING

The Kerr nonlinearity also gives rise to the most frequently studied parametric nonlinear optical interaction in silicon-based photonics: four-wave mixing (FWM). In essence, FWM is simply the spectral representation of self-phase modulation. In FWM, two photons are annihilated to produce two new photons, with no energy lost to nonradiative processes thereby making it a parametric process. The relationship between the waves is represented by: $\omega_1 +$

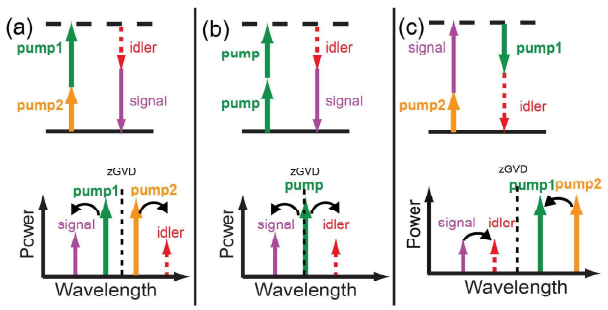

Fig. 4. *Schematic energy level diagrams (top) and spectra (bottom) of different FWM configurations, the arrows show the energy transfer directions: (a) nondegenerate FWM; (b) pump-degenerate FWM; and (c) FWM-BS.*

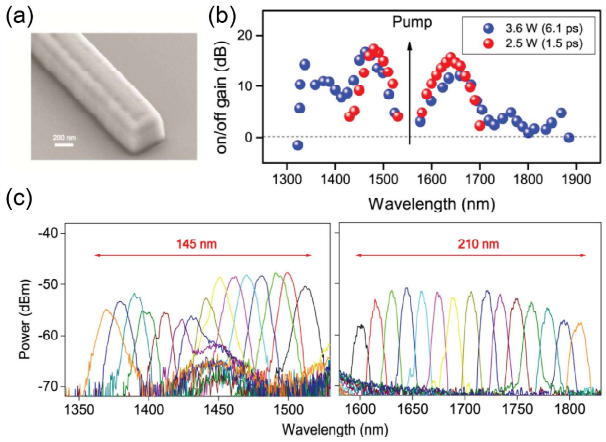

Fig. 5. *Experimental results of optical parametric amplifier and oscillator using an a-Si:H waveguide: (a) scanning electron microscopy image of the a-Si:H waveguide; (b) on/off amplification of the a-Si:H waveguide using a 1.5-ps pump with peak power of 2.5 W and 6.1-ps pump with peak power of 3.6 W; and c) overlaid tuning spectra of the oscillation mode of the OPO at short wavelength side (1370 nm ~ 1515 nm), and long wavelength side (1600 nm ~ 1810 nm) for a 1558-nm pump laser. Figure reproduced with permission from [83], ©2015 OSA.*

$\omega_2 = \omega_3 + \omega_4$, where ω_i denotes the frequency of each involved wave. This interaction can be realized in several different configurations such as those depicted in Fig. 4. As dispersion is critical to efficient FWM, the approximate zero group velocity dispersion (zGVD) locations that would enable ideal phase matching are indicated for each interaction.

Shown in Fig. 4(a) is the conventional nondegenerate FWM configuration, in which four waves at different wavelengths are involved; as depicted in the optical spectrum with solid lines, two high power waves (pump1 and pump2) and a relatively low power wave (signal) are input into the nonlinear element, and an idler (red dashed line) is generated due to the nondegenerate FWM process. In this case, a pump1 photon and a pump2 photon are converted to a signal photon and an idler photon, and hence $\omega_{P1} + \omega_{P2} = \omega_s + \omega_i$. A specific FWM case is depicted in Fig. 4(b) when the two pumps are at the same wavelength (degenerate); this configuration is called pump-degenerate FWM. In this configuration, two pump photons at the same frequency can be used to create a signal and idler photon at different wavelengths: $\omega_{P1} + \omega_{P1} = \omega_s + \omega_i$. In both processes, the energy is transferred from the pump waves to the signal and idler waves, and these processes have enabled a variety of applications such as broadband signal amplification [5], [28], [29], [35], [72] and wavelength conversion [14], [22], [26], [28], [49], [51], [52], as well as quantum applications including photon-pair generation [73]–[82]. For example, through proper phase matching of a highly nonlinear a-Si:H waveguide, signal amplification is achieved over a 500-nm bandwidth in the telecommunications wavelength range and beyond as shown in Fig. 5(a) and (b) [83]. Placing this broad-bandwidth gain device within a dispersive optical cavity then enables optical parametric oscillation (OPO) and thus a coherent source whose output can be tuned over a range of wavelengths comparable to the amplification bandwidth, as shown in Fig. 5(c).

The FWM process can also be used for wavelength conversion, where light at one wavelength is converted to another wavelength. In c-Si photonic devices broad bandwidth (837 nm) wavelength conversion with modest CW conversion efficiencies of -20 dB [84], and CW conversion efficiencies up to -1 dB with active carrier removal structures (p–i–n diodes) over modest bandwidths ~12 nm [49] or -4.4 dB with a similar bandwidth [51] have been achieved at telecommunications wavelengths.

The third FWM configuration shown in Fig. 4(c) is FWM-Bragg scattering (FWM-BS). In this configuration, a photon from a high-power pump wave and a photon from a low power signal wave are annihilated to create an idler photon and a pump photon at a different frequency: $\omega_{P2} + \omega_s = \omega_{p1} + \omega_i$. Since the power in the signal is lower than a typical pump would be, depletion of the signal wave can be significant, and can be exploited for various applications including optical isolation [85] and logic gates [86]. Additionally, this process is attractive for low-noise applications, such as quantum signal processing [13], [87]–[91], since the wavelength conversion that occurs does not amplify any vacuum fluctuations as the power in the sideband (including the signal and idlers) remains constant.

V. APPLICATIONS

Nonlinear silicon-based photonics are impacting several important application domains. Similar to traditional silicon photonics, the most prevalent applications relate to communications. Additionally, nonlinear silicon photonic devices are being demonstrated with applications in all-optical computing, metrology, and security. Some notable works in these areas are highlighted below.

A. Communications

Nonlinear optical interactions have the ability to manipulate extremely high capacity data signals for communications. In silicon-based waveguides, demonstrations of all-

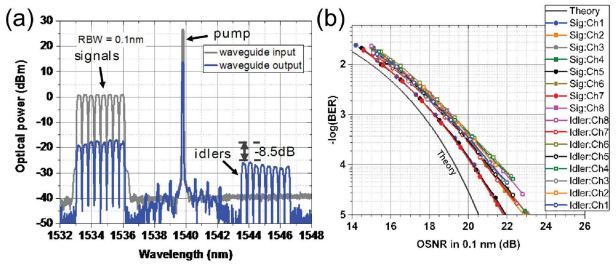

Fig. 6. *(a) Input and output optical spectra of the wavelength conversion process for the 1.024-Tb/s data. (b) Bit error rate (BER) versus optical signal-to-noise ratio (OSNR) measurements of the 8 × 32-GBd single-polarization 16QAM data showing the BER performances of the back-to-back signals (i.e., without the wavelength converter) and the wavelength-converted idlers of all eight channels. Figure reprinted with permission from [52], ©2017 OSA.*

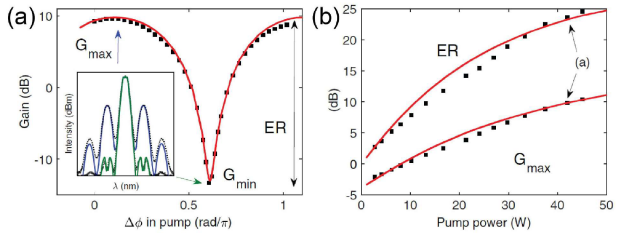

Fig. 8. *(a) Experimental (squares) and numerically calculated (solid line) phase-sensitive gain of the signal wave at peak pump power of 42 W, as a function of pump phase detuning ($\Delta\phi$) with a periodicity of π. Inset: simulated results (blue and green) agree with the measured output spectra at the maximum ($G_{\max}$) and minimum ($G_{\min}$) gains, respectively. (b) Both the maximum gain and ER increase with pump power without reaching saturation. Figure reproduced with permission from [97], ©2017 OSA.*

optical signal processing have included wavelength conversion of high-data-rate communication signals [52], [92], [93]. For example, wavelength conversion is achieved on wavelength division multiplexed (WDM) signals up to 1.024 Tb/s with efficiencies of −8.5 dB in c-Si waveguides that exploit reverse-biased p–i–n junctions for carrier removal [52]. This demonstration is highlighted in Fig. 6 where the spectrum of the waves as well as the bit-error-rate plots are shown.

Optical time division multiplexing (OTDM) is another approach to exploiting the large bandwidth afforded through the use of optical signals. In such a communication scheme, the high data rate signal must be demultiplexed into multiple, lower data-rate optical channels for parallel detection at these lower rates. In a-Si:H, 160-to-10-Gb/s OTDM demultiplexing was achieved with ∼50 mW of peak pump powers [94] and in c-Si with ∼500 mW of peak pump powers [95]. As highlighted in Fig. 7, OTDM of extremely high data rate signals (1.28-Tb/s–10-Gb/s OTDM) has been achieved in c-Si with error-free operation [96].

As a signal transmits in the optical channel, distortions can be induced by dispersion, nonlinearity, and noise. Therefore, high-speed and broadband signal regeneration techniques are highly desired in a communication system. As the FWM process is naturally dependent on the phase relationship between the signals, the process is often exploited in a technique called phase sensitive amplification (PSA) where signals can be regenerated to overcome the quantum noise limit. PSA utilizing either a pump- or signal-idler-degenerate FWM scheme has been demonstrated in a number of silicon-based platforms including net gain of 10.4 dB and extinction ratio (ER) of 24.6 dB in Hydex at repetition rates of ∼17 MHz [97] as shown in Fig. 8. In other silicon-based platforms, up to 20 dB of ER at CW operation in c-Si with p–i–n [50] and ER of 11.7 dB at 90 MHz operation and 1.6 dB at CW operation in a-Si:H waveguides [98]. Phase regeneration of a 10-Gb/s DPSK signals has been proven based on PSA in a c-Si waveguide [50]. Besides FWM-based PSA, other nonlinear techniques like SPM [99] and XPM [71] can also be utilized for signal regeneration, as mentioned previously.

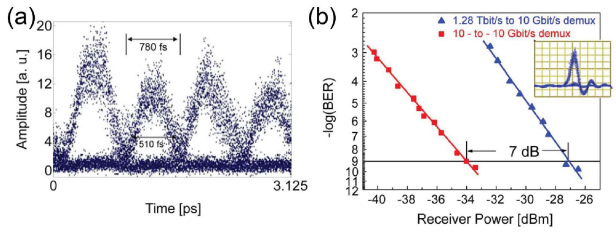

Fig. 7. *(a) Clear eye diagrams of 1.28-Tb/s waveform from the Si-based optical sampling. (b) BER performance of 1.28-Tb/s–10-Gb/s demultiplexing. Figure reprinted with permission from [96], ©2011 IEEE.*

In addition to WDM, OTDM and signal regeneration applications, FWM-based wavelength conversion has been utilized in silicon platforms for communications applications such as multicasting [100]–[102], tunable delays through optical phase conjugation [103], [104], as well as signal regeneration [105].

B. All-Optical Computing

The utilization of all-optical signal processing is not limited to the analog domain, and recent demonstrations have shown the ability to achieve high data-rate digital logic operations. However, today's electronics operate at extremely low power, making it difficult to envision scenarios where optics could find a place in computation. Although nonlinear optical interactions are being pushed to lower and lower powers (approximately a milliwatt), such powers are still quite large compared to electronics. However, all-optical logic gates can operate at significantly higher serial rates than electronics. Thus integrated nonlinear optical computing is better suited to applications where high-speed serial information already exists in the optical domain and can be processed at the native data rate without conversion between the optical and electrical domains. In such preprocessing applications, computational blocks such as flip-flops, adders, and logic blocks for encryption are of significant interest.

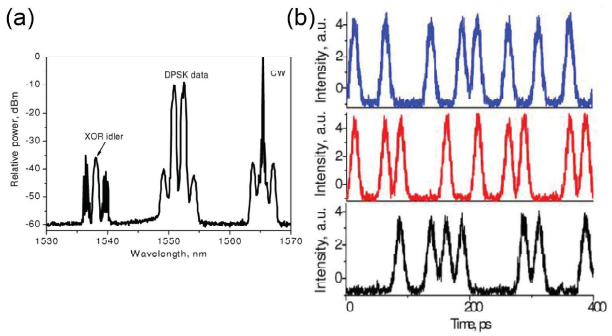

Fig. 9. *(a) Output optical spectrum for XOR logic gate. (b) Pulse traces corresponding to the 40-Gb/s input DPSK signals (top and middle) and the output 40-Gb/s idler (bottom), representing the XOR logic output. Figure reproduced with permission from [106], ©2011 OSA.*

A number of research efforts in the direction of all-optical computing have been demonstrated in silicon-based platforms utilizing ultrafast parametric nonlinear interactions [106]–[110]. In [106], an all-optical XOR logic operation for 40-Gb/s differential phase-shift keyed (DPSK) data signals in the telecom C-band is demonstrated in a c-Si nanowire based on FWM, with a system penalty of ~3.0 dB and ~4.3 dB at 10^{-9} BER, as shown in Fig. 9. In [110], 1.25-Gb/s all-optical NAND/AND logic functions are realized for optical waves encoded in ON/OFF keying (OOK) format, utilizing FWM-BS in an a-Si:H waveguide, as depicted in Fig. 10. These demonstrations represent a further step toward the realization of integrated high-speed all-optical computing via silicon photonics.

C. Metrology

Mid-infrared (mid-IR) optical systems promise to have applications in industrial and environmental monitoring [111], explosives detection [112], as well as chemical and biomolecular sensing [113]. However, room temperature low-noise mid-IR detection is a substantial challenge due to the narrow bandgap of the semiconductors required for photodetection. To this end, mid-IR to telecom-band frequency translation is a technique that can avoid such

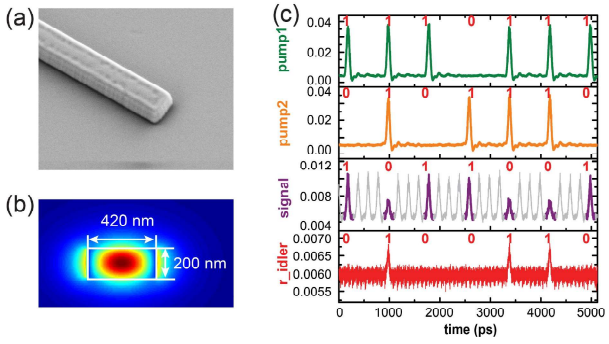

Fig. 10. *The 1.25-Gb/s NAND/AND logic gate. (a) SEM image of the a-Si:H waveguide. (b) Simulated TE mode profile. (c) Time domain pulse traces corresponding to the inputs (green and orange), NAND logic output (purple), and AND logic output (red). Figure reprinted from [110].*

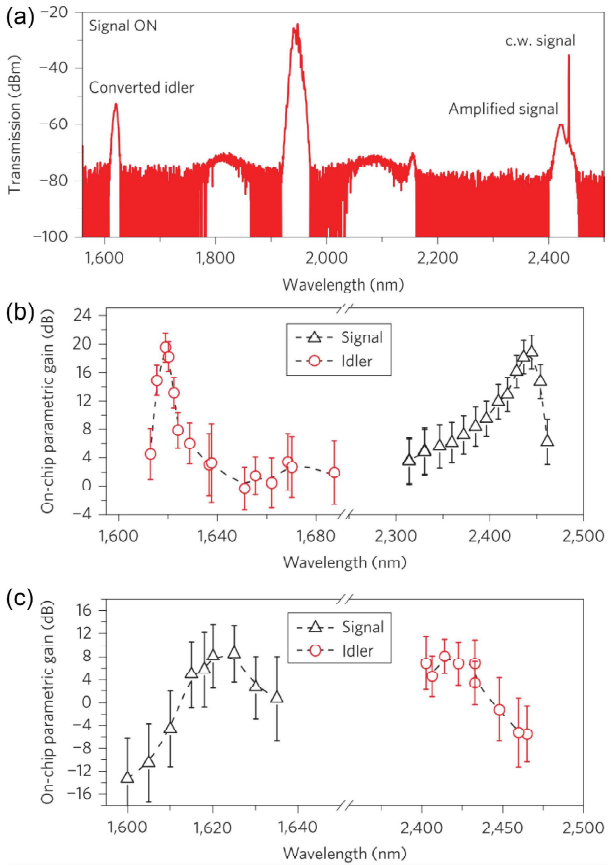

Fig. 11. *Spectral translation using FWM. (a) Output transmission spectrum with pump operating at 1946 nm and signal at 2440 nm; wavelength-resolved on-chip spectral translation efficiency and parametric signal gain with (b) a mid-IR input signal and (c) a telecom-band input signal. Figure reprinted with permission from [114], ©2012 Macmillan Publishers Limited.*

issues. In [114], efficient FWM in a silicon waveguide is accomplished with discrete band phase-matching to facilitate the conversion of a signal at 2440 nm (mid-IR) to an idler at 1620 nm (telecom band). This demonstration shows spectral translation across a span of 62 THz with simultaneous parametric translation gain as high as 19 dB (see Fig. 11). A variety of other work on mid-IR photonics in silicon-based devices has been reported [31], [113], [115], [116], indicating that silicon photonics can play an important role in both the telecom-band and mid-IR regimes.

Parametric nonlinear optical interactions in resonant cavities with the proper gain and dispersion conditions can be utilized to achieve optical frequency comb generation. An optical frequency comb is a coherent source consisting of a series of discrete, equally spaced frequencies (comb teeth) in its spectrum. Frequency combs have significant applications in various areas of metrology including optical clockwork [117], [118] and precision spectroscopy (using optical frequency synthesizers) [117], [119]. Recently, a highly precise optical frequency synthesizer utilizing two integrated combs (a SiN_x microresonator and a SiO_2 microresonator), a

heterogeneously integrated III–V/Si tunable laser as well as other controlling and monitoring components have been reported [120], representing an important step toward fully integrated frequency synthesizers. Furthermore, creating frequency combs with compact, low-power integrated photonic devices makes them accessible to a broad array of classical applications such as remote chemical/biological sensing [113], dual-comb spectroscopy [121], RF and microwave signal processing [122], and optical coherent communications [123], as well as quantum applications including the generation of photon pairs [82], [124] and multiphoton entangled quantum states [125].

Silicon-based photonic devices such as SiN_x and Hydex where nonlinear interactions can occur with net CW gain, and dispersion engineering provide an ideal platform for frequency comb generation, and a wealth of research has been focused on developing and studying these devices [82], [113], [122]–[129]. The first integrated octave-spanning frequency comb generation was demonstrated in a SiN_x microring resonator, showing a wide spectral output spanning 128 THz with a line spacing of 226 GHz [127], as depicted in Fig. 12(a). Recently, integrated phase-coherent frequency combs have been realized in the soliton regime [130], as shown in Fig. 12(b). Due to the reduced nonlinear loss in the mid-IR range, c-Si microresonator-based combs have also been demonstrated [113] and employed for spectroscopy [121]. These investigations pave the way for the realization of stable phase-locked frequency combs on-chip. Research on frequency combs has been comprehensively reviewed in [4] and [131].

D. Security

Information security is always of great concern in both communication and data storage systems. Ever since the early days of communication, the necessity of protecting the confidentiality of correspondence and detecting tampering has been critical. Today, with the growth of the Internet of Things, it is increasingly important to develop reliable methods to guarantee the security and privacy of information [132]. In this section, we will briefly discuss some promising methods for secure optical communications and authentication employing silicon photonics.

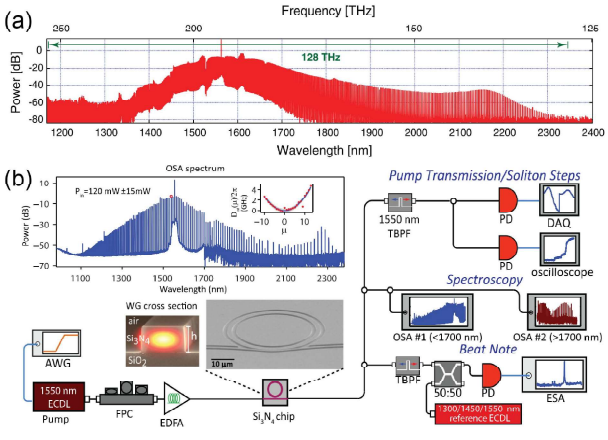

Fig. 12. *(a) Experimental octave-spanning comb generated in a silicon nitride microring. Figure reproduced with permission from [127], ©2011 OSA. (b) Experimental setup and comb generation in the soliton regime in a silicon nitride microring. Figure reproduced with permission from [130], ©2017 OSA.*

1) Quantum Communications: If information is communicated in as small an information carrying unit as physically possible (e.g., at the single photon level), detecting the presence of eavesdroppers is feasible. This concept of quantizing communication signals into individual particles has given rise to the field of quantum communications. Many such proposed schemes also rely upon the quantum concept that once a signal is measured, its properties are altered in some way (a particle which statistically existing in one basis is forced onto the basis of the measurement technique) and therefore eavesdropping can be detected through the statistical likelihood of errors.

A quantum communication network for secure communications requires more than just interconnects by which signals are sent. The first pivotal element for quantum communication systems is efficient sources of photons satisfying the requirements of anti-bunching (individual photons separated in time without overlap) and/or entanglement (the quantum state of one photon is dependent on the states of others). A great deal of work has demonstrated the potential of generating single and photon pair sources utilizing parametric nonlinear effects in silicon-based photonic devices [76]–[82], [124], [125], [133]–[135]. As a recent example, photons generated via FWM in a silicon waveguide from four temporal modes have been multiplexed temporally to achieve 100% enhancement to the single-photon output probability [134], as shown in Fig. 13(a); and photon indistinguishability is confirmed by a fourfold Hong–Ou–Mandel (HOM) quantum interference with a 91± 16% visibility after subtracting multiphoton noise due to high pump power [see Fig. 13(c)].

Other essential components for a quantum network include signal repeaters and processors. In order for such devices to be practical, processing must be achieved with low power and low noise. Integrated silicon photonics provides a means toward scalable quantum communication networks since it can reduce the power requirement of optical processing interactions. For example, researchers have demonstrated efficient low-noise frequency conversion at single-photon level in a SiN_x microring resonator via FWM-BS [90]. In addition, silicon photonics also shows great potential for high-speed quantum key distribution [136]. These reports indicate the potential for integrated silicon-based photonic devices for quantum communication networks.

2) Photonic Physically Unclonable Functions: The manner in which light can interact with a material can be attributed

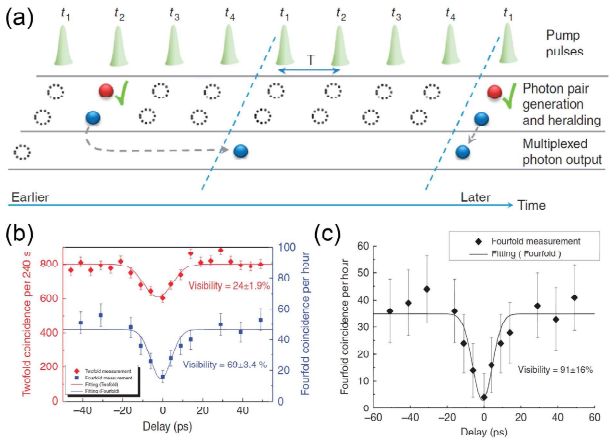

Fig. 13. *Demonstration of temporal multiplexing of indistinguishable single photons. (a) Principle of operation. (b) Visibility of twofold and fourfold measurements. (c) Fourfold HOM dip visibility after subtracting multiphoton noise. Figure reproduced from [133].*

to many different processes, both linear and nonlinear. Linear interactions include refraction, scattering, diffraction, absorption, etc., and can occur due to nanometer-scale perturbations in materials or interfaces. Although we have focused on only a few, there are also a great deal of nonlinear interactions available in an integrated photonic platform. This rich array of phenomena can be exploited to create very information-dense optical interactions in integrated photonic devices. Devices with such complex behavior can serve as physical keys for security applications such as authentication and encryption. In [137], a silicon photonic physical unclonable function based on ultrafast nonlinear optical interactions in a chaotic c-Si microcavity is demonstrated. Due to the complex nonlinear interactions in the cavity, the device presents a highly unpredictable, yet deterministic and ultrafast response to data encoded optical pulses. This response behavior can serve as a unique "fingerprint" of the device and as a source of private information for the device's holder. The potential of using this device for information security is demonstrated via the challenge-response authentication experiments, in which the device serves as an authentication token (a hardware device that is used to prove an identity and authorize access to a protected resource), as shown in Fig. 14. Furthermore, the device is experimentally demonstrated to be unclonable due to unavoidable fabrication variations. These devices have also more recently been extended to serve as sources of key material for data encryption [138].

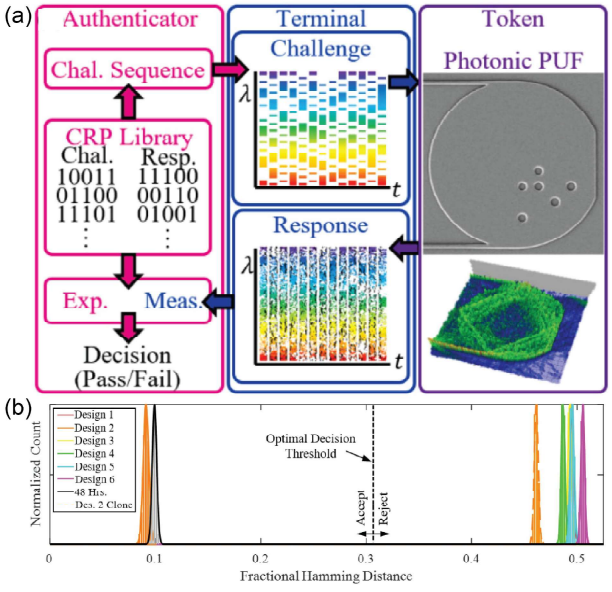

Fig. 14. *Silicon photonic physical unclonable function (PUF). (a) Authentication system with the silicon photonic physical unclonable function as the token. (b) Experimental performance showing that only the real device at time = 0(solid orange) and 48 h later (black) passes the authentication test. Figure reproduced with permission from [137], ©2017 OSA.*

VI. CONCLUSION

In this review, we have discussed recent progress in nonlinear silicon-based photonic devices. As shown in Table 1, the versatility of silicon-based materials provides a suite of material options to choose from while engineering the optimal device for a specific application. Crystalline silicon's relatively high nonlinearity as well as the ability to incorporate loss-reduction techniques (such as p–i–n diodes) have enabled a number of exciting demonstrations in both the telecommunication and mid-IR regimes. Silicon nitride and Hydex have extremely low linear losses and negligible nonlinear losses, however with a tradeoff of significantly lower nonlinearities compared to their semiconductor counterparts. Still, the low loss properties of silicon nitride and Hydex provide a powerful platform to create microresonators with extremely high quality factors, thereby producing remarkably efficient nonlinear interactions such as frequency conversion, optical parametric oscillation, and frequency comb generation. Hydrogenated amorphous silicon has been demonstrated with the highest nonlinear refractive index that is one order of magnitude larger than c-Si and an improved nonlinear FOM. These properties allow hydrogenated amorphous silicon devices to operate at very low power and high efficiencies.

In addition to the materials discussed in this paper, great effort has been made to develop other silicon-based materials such as silicon-rich nitride [66], [139]–[141] and silicon germanium (SiGe) [142]–[146], mainly due to their flexibility to tune the refractive index, bandgap, and other optical properties by varying the element concentrations. Research on silicon-rich nitride is aimed to increase the refractive index and nonlinearity of silicon nitride while maintaining low 2PA; reports have shown its potential applications in wavelength conversion [140]

and supercontinuum generation [66]. Silicon germanium alloys have attracted tremendous attention for near- and mid-IR applications [143], [145], owing to their larger refractive index and nonlinear coefficient than c-Si in the near- and mid-IR wavelength ranges.

To date, the silicon-based platform for nonlinear optics has enabled a variety of exciting applications in areas such as communications, all-optical computing, metrology, and security and in both the classical and quantum domains. An intriguingly recent trend is the possibility of combining the unique merits of these materials into heterogeneously integrated devices with superior overall performance [147], [148]. Overall, the high nonlinear performance and inherent compatibility with mature CMOS fabrication techniques of silicon photonic devices show great promise for realizing all-optical photonic systems with low cost, small footprint, and low power consumption. ■

REFERENCES

[1] E. Garmire, "Nonlinear optics in daily life," *Opt. Express*, vol. 21, no. 25, pp. 30532–30544, 2013.

[2] J. Leuthold, C. Koos, and W. Freude, "Nonlinear silicon photonics," *Nature Photon.*, vol. 4, pp. 535–544, Jul. 2010.

[3] D. J. Moss, R. Morandotti, A. L. Gaeta, and M. Lipson, "New CMOS-compatible platforms based on silicon nitride and Hydex for nonlinear optics," *Nature Photon.*, vol. 7, pp. 597–607, Aug. 2013.

[4] M. Borghi, C. Castellan, S. Signorini, A. Trenti, and L. Pavesi, "Nonlinear silicon photonics," *J. Opt.*, vol. 19, no. 9, 2017.

[5] M. A. Foster, A. C. Turner, J. E. Sharping, B. S. Schmidt, M. Lipson, and A. L. Gaeta, "Broad-band optical parametric gain on a silicon photonic chip," *Nature*, vol. 441, pp. 960–963, Jun. 2006.

[6] C. Koos, L. Jacome, C. Poulton, J. Leuthold, and W. Freude, "Nonlinear silicon-on-insulator waveguides for all- optical signal processing," *Opt. Express*, vol. 15, no. 10, pp. 5976–5990, 2007.

[7] C. Monat *et al.*, "Four-wave mixing in slow light engineered silicon photonic crystal waveguides," *Opt. Express*, vol. 18, no. 22, pp. 22915–22927, 2010.

[8] J. F. McMillan, M. Yu, D.-L. Kwong, and C. W. Wong, "Observation of four-wave mixing in slow-light silicon photonic crystal waveguides," *Opt. Express*, vol. 18, no. 15, pp. 15484–15497, 2010.

[9] J. S. Levy, A. Gondarenko, M. A. Foster, A. C. Turner-Foster, A. L. Gaeta, and M. Lipson, "CMOS-compatible multiple-wavelength oscillator for on-chip optical interconnects," *Nature Photon.*, vol. 4, pp. 37–40, Dec. 2010.

[10] M. Ferrera *et al.*, "Low-power continuous-wave nonlinear optics in doped silica glass integrated waveguide structures," *Nature Photon.*, vol. 2, pp. 737–740, Nov. 2008.

[11] L. Razzari *et al.*, "CMOS-compatible integrated optical hyper-parametric oscillator," *Nature Photon.*, vol. 4, pp. 41–45, Dec. 2010.

[12] B. Kuyken *et al.*, "Nonlinear properties of and nonlinear processing in hydrogenated amorphous silicon waveguides," *Opt. Express*, vol. 19, no. 26, pp. B146–B153, Dec. 2011.

[13] K. Li, H. Sun, and A. C. Foster, "Four-wave mixing Bragg scattering in hydrogenated amorphous silicon waveguides," *Opt. Lett.*, vol. 42, no. 8, pp. 1488–1491, 2017.

[14] K.-Y. Wang and A. C. Foster, "Ultralow power continuous-wave frequency conversion in hydrogenated amorphous silicon waveguides," *Opt. Lett.*, vol. 37, no. 8, pp. 1331–1333, Apr. 2012.

[15] C. Grillet *et al.*, "Amorphous silicon nanowires combining high nonlinearity, FOM and optical stability," *Opt. Express*, vol. 20, no. 20, pp. 22609–22615, 2012.

[16] C. Lacava, P. Minzioni, E. Baldini, L. Tartara, J. M. Fedeli, and I. Cristiani, "Nonlinear characterization of hydrogenated amorphous silicon waveguides and analysis of carrier dynamics," *Appl. Phys. Lett.*, vol. 103, no. 14, p. 141103, 2013.

[17] K. Li and A. C. Foster, "Nonlinear optics in hydrogenated amorphous silicon," *IEEE J. Sel. Topics Quantum Electron.*, vol. 24, no. 6, pp. 1–12, Dec. 2018.

[18] M. Stutzmann, W. B. Jackson, and C. C. Tsai, "Light-induced metastable defects in hydrogenated amorphous silicon: A systenmatic study," *Phys. Rev. B, Condens. Matter*, vol. 32, no. 1, pp. 24–47, 1985.

[19] A. Kolstrokodziej, "Staebler-Wronski effect in amorphous silicon and its alloys," *Opto-Electron. Rev.*, vol. 12, no. 1, pp. 21–32, 2004.

[20] *Corning SMF-28 Ultra Optical Fiber, Datasheet*, 2014.

[21] *Highly Non-Linear Fiber Module OFS Specification Sheet, Datasheet*, OFS, 2009.

[22] M. A. Foster, A. C. Turner, R. Salem, M. Lipson, and A. L. Gaeta, "Broad-band continuous-wave parametric wavelength conversion in silicon nanowaveguides," *Opt. Express*, vol. 15, no. 20, pp. 12949–12958, 2007.

[23] J. M. Díaz, J. B. Nadal, D. Vukovic, F. Da Ros, E. Palushani, and C. Peucheret, "A comparison of nonlinear media for parametric all-optical signal processing," in *Proc. IEEE Photon. Conf.*, Bellevue, WA, USA, Sep. 2013, pp. 679–680.

[24] D. Dimitropoulos, V. Raghunathan, R. Claps, and B. Jalali, "Phase-matching and nonlinear optical processes in silicon waveguides," *Opt. Express*, vol. 12, no. 1, pp. 149–160, 2004.

[25] A. C. Turner *et al.*, "Tailored anomalous group-velocity dispersion in silicon channel waveguides," *Opt. Express*, vol. 14, no. 10, pp. 4357–4362, 2006.

[26] Q. Lin, J. Zhang, P. M. Fauchet, and G. P. Agrawal, "Ultrabroadband parametric generation and wavelength conversion in silicon waveguides," *Opt. Express*, vol. 14, no. 11, pp. 4786–4799, 2006.

[27] L. Yin, Q. Lin, and G. P. Agrawal, "Dispersion tailoring and soliton propagation in silicon waveguides," *Opt. Lett.*, vol. 31, no. 9, pp. 1295–1297, 2006.

[28] M. R. E. Lamont, C. M. de Sterke, and B. J. Eggleton, "Dispersion engineering of highly nonlinear As2S3 waveguides for parametric gain and wavelength conversion," *Opt. Express*, vol. 15, no. 15, pp. 9458–9463, 2007.

[29] K.-Y. Wang and A. C. Foster, "GHz-rate optical parametric amplifier in hydrogenated amorphous silicon," *J. Opt.*, vol. 17, no. 9, p. 094012, 2015.

[30] F. Leo, S.-P. Gorza, S. Coen, B. Kuyken, and G. Roelkens, "Coherent supercontinuum generation in a silicon photonic wire in the telecommunication wavelength range," *Opt. Lett.*, vol. 40, no. 1, pp. 123–126, 2015.

[31] H. Sun, K.-Y. Wang, R. Salem, P. Fendel, and A. C. Foster, "Coherent mid-IR supercontinuum generation in a hydrogenated amorphous silicon waveguide," in *Proc. Conf. Laser Electr-optics*, 2015, Paper SM1P.6.

[32] J. Safioui *et al.*, "Supercontinuum generation in hydrogenated amorphous silicon waveguides at telecommunication wavelengths," *Opt. Express*, vol. 22, no. 3, pp. 3089–3097, Feb. 2014.

[33] Y. Okawachi *et al.*, "Bandwidth shaping of microresonator-based frequency combs via dispersion engineering," *Opt. Lett.*, vol. 39, no. 12, pp. 3535–3538, Jun. 2014.

[34] J. B. Driscoll *et al.*, "Width-modulation of Si photonic wires for quasi-phase-matching of four-wave-mixing: Experimental and theoretical demonstration," *Opt. Express*, vol. 20, no. 8, pp. 9227–9242, 2012.

[35] S. Lavdas, S. Zhao, J. B. Driscoll, R. R. Grote, R. M. Osgood, Jr., and N. C. Panoiu, "Wavelength conversion and parametric amplification of optical pulses via quasi-phase-matched four-wave mixing in long-period Bragg silicon waveguides," *Opt. Lett.*, vol. 39, no. 13, pp. 4017–4020, 2014.

[36] D. D. Hickstein *et al.*, "Quasi-phase-matched supercontinuum generation in photonic waveguides," *Phys. Rev. Lett.*, vol. 120, p. 053903, 2018.

[37] A. C. Turner-Foster *et al.*, "Ultrashort free-carrier lifetime in low-loss silicon nanowaveguides," *Opt. Express*, vol. 18, no. 4, pp. 3582–3591, Feb. 2010.

[38] T. Baehr-Jones, M. Hochberg, and A. Scherer, "Photodetection in silicon beyond the band edge with surface states," *Opt. Express*, vol. 16, pp. 1659–1668, Feb. 2008.

[39] K. Ikeda, Y. Shen, and Y. Fainman, "Enhanced optical nonlinearity in amorphous silicon and its application to waveguide devices," *Opt. Express*, vol. 15, no. 26, pp. 17761–17771, 2007.

[40] K. Narayanan and S. F. Preble, "Optical nonlinearities in hydrogenated-amorphous silicon waveguides," *Opt. Express*, vol. 18, no. 9, pp. 8998–9005, 2010.

[41] L. Yin and G. P. Agrawal, "Impact of two-photon absorption on self-phase modulation in silicon waveguides," *Opt. Lett.*, vol. 32, no. 14, pp. 2031–2033, Jul. 2007.

[42] X. Gai, D.-Y. Choi, and B. Luther-Davies, "Negligible nonlinear absorption in hydrogenated amorphous silicon at 1.55 μm for ultra-fast nonlinear signal processing," *Opt. Express*, vol. 22, no. 8, pp. 9948–9958, Apr. 2014.

[43] X. Zeng, T. Tran, J. S. Pelc, D. Kielpinski, and R. G. Beausoleil, "Effects of non-instantaneous nonlinear absorption in hydrogenated amorphous silicon," in *Proc. Conf. Laser Electro-Opt.*, 2016, Paper SM3R.6.

[44] J. J. Wathen, V. R. Pagán, R. J. Suess, K.-Y. Wang, A. C. Foster, and T. E. Murphy, "Non-instantaneous optical nonlinearity of an a-Si:H nanowire waveguide," *Opt. Express*, vol. 22, no. 19, pp. 22730–22742, 2014.

[45] K. Fukutani *et al.*, "Band gap tuning of a-Si:H from 1.55 eV to 2.10 eV by intentionally promoting structural relaxation," *J. Non-Cryst. Solids*, vols. vol. 227–vol. 230, pp. 63–67, 1998.

[46] F. Da Ros *et al.*, "Dual-polarization wavelength conversion of 16-QAM signals in a single silicon waveguide with a lateral p-i-n diode [Invited]," *Photon. Res.*, vol. 6, no. 5, pp. B23–B29, 2018.

[47] L.-D. Haret *et al.*, "Schottky MSM junctions for carrier depletion in silicon photonic crystal microcavities," *Opt. Exp.*, vol. 21, no. 8, pp. 10324–10334, 2013.

[48] Y. Ding, H. Hu, H. Ou, L. K. Oxenløwe, and K. Yvind, "Effective carrier sweepout in a silicon waveguide by a metal-semiconductor-metal structure," in *Proc. Conf. Lasers Electro-Opt.*, 2015, Paper SM1I.5.

[49] A. Gajda *et al.*, "Highly efficient CW parametric conversion at 1550 nm in SOI waveguides by reverse biased p-i-n junction," *Opt. Express*,

vol. 20, no. 12, pp. 13100–13107, 2012.
[50] F. Da Ros *et al.*, "Phase regeneration of DPSK signals in a silicon waveguide with reverse-biased p-i-n junction," *Opt. Express*, vol. 22, no. 5, pp. 5029–5036, Feb. 2014.
[51] J. R. Ong, R. Kumar, R. Aguinaldo, and S. Mookherjea, "Efficient CW four-wave mixing in silicon-on-insulator micro-rings with active carrier removal," *IEEE Photon. Technol. Lett.*, vol. 25, no. 17, pp. 1699–1702, Sep. 2013.
[52] I. Sackey *et al.*, "1.024 Tb/s wavelength conversion in a silicon waveguide with reverse-biased p-i-n junction," *Opt. Express*, vol. 25, no. 18, pp. 21229–21240, 2017.
[53] R. Hezel and K. Jaeger, "Low-temperature surface passivation of silicon for solar cells," *J. Electrochem. Soc.*, vol. 136, no. 2, pp. 518–523, 1989.
[54] H. Mäckel and R. Lüdemann, "Detailed study of the composition of hydrogenated SiNx layers for high-quality silicon surface passivation," *J. Appl. Phys.*, vol. 92, no. 5, pp. 2602–2609, 2002.
[55] G. Agostinelli *et al.*, "Very low surface recombination velocities on p-type silicon wafers passivated with a dielectric with fixed negative charge," *Solar Energy Mater. Solar Cells*, vol. 90, pp. 3438–3443, Nov. 2006.
[56] J. S. Pelc, K. Rivoire, S. Vo, C. Santori, D. A. Fattal, and R. G. Beausoleil, "Picosecond all-optical switching in hydrogenated amorphous silicon microring resonators," *Opt. Express*, vol. 22, no. 4, pp. 3797–3810, 2014.
[57] B. Tuttle and J. B. Adams, "Structure, dissociation, and the vibrational signatures of hydrogen clusters in amorphous silicon," *Phys. Rev. B, Condens. Matter*, vol. 56, no. 8, pp. 4565–4572, Aug. 1997.
[58] O. Boyraz, T. Indukuri, and B. Jalali, "Self-phase-modulation induced spectral broadening in silicon waveguides," *Opt. Express*, vol. 12, no. 5, pp. 829–834, 2004.
[59] L. Yin, Q. Lin, and G. P. Agrawal, "Soliton fission and supercontinuum generation in silicon waveguides," *Opt. Lett.*, vol. 32, no. 4, pp. 391–393, Feb. 2007.
[60] F. Leo *et al.*, "Dispersive wave emission and supercontinuum generation in a silicon wire waveguide pumped around the 1550 nm telecommunication wavelength," *Opt. Lett.*, vol. 39, no. 12, pp. 3623–3626, Jun. 2014.
[61] B. Kuyken, X. Liu, R. M. Osgood, Jr., R. Baets, G. Roelkens, and W. M. J. Green, "Mid-infrared to telecom-band supercontinuum generation in highly nonlinear silicon-on-insulator wire waveguides," *Opt. Express*, vol. 19, no. 21, pp. 20172–20181, Oct. 2011.
[62] N. Singh *et al.*, "Midinfrared supercontinuum generation from 2 to 6 μm in a silicon nanowire," *Optica*, vol. 2, no. 9, pp. 797–802, 2015.
[63] R. Halir, Y. Okawachi, J. S. Levy, M. A. Foster, M. Lipson, and A. L. Gaeta, "Ultrabroadband supercontinuum generation in a CMOS-compatible platform," *Opt. Lett.*, vol. 37, no. 10, pp. 1685–1687, May 2012.
[64] A. R. Johnson *et al.*, "Octave-spanning coherent supercontinuum generation in a silicon nitride waveguide," *Opt. Lett.*, vol. 40, no. 21, pp. 5117–5120, 2015.
[65] H. Zhao *et al.*, "Visible-to-near-infrared octave spanning supercontinuum generation in a silicon nitride waveguide," *Opt. Lett.*, vol. 40, no. 10, pp. 2177–2180, 2015.
[66] X. Liu *et al.*, "Octave-spanning supercontinuum generation in a silicon-rich nitride waveguide," *Opt. Lett.*, vol. 41, no. 12, pp. 2719–2722, 2016.
[67] M. A. G. Porcel *et al.*, "Two-octave spanning supercontinuum generation in stoichiometric silicon nitride waveguides pumped at telecom wavelengths," *Opt. Express*, vol. 25, no. 2, pp. 1542–1554, 2017.
[68] U. D. Dave, S. Uvin, B. Kuyken, S. Selvaraja, F. Leo, and G. Roelkens, "Telecom to mid-infrared spanning supercontinuum generation in hydrogenated amorphous silicon waveguides using a Thulium doped fiber laser pump source," *Opt. Express*, vol. 21, no. 26, pp. 32032–32039, 2013.
[69] Y. Zhang *et al.*, "Cross-phase modulation-induced spectral broadening in silicon waveguides," *Opt. Express*, vol. 24, no. 1, pp. 443–451, 2016.
[70] S. Suda *et al.*, "High-bit-rate optical switching based on XPM in silicon waveguides," in *Proc. Int. Conf. Photon. Switching*, 2009, pp. 1–2.
[71] A. S. Jensen, H. Hu, H. Ji, M. Pu, L. H. Frandsen, and L. K. Oxenløwe, "All-optical 40 Gbit/s regenerative wavelength conversion based on cross-phase modulation in a silicon nanowire," in *Proc. Int. Conf. Photon. Switching*, 2013, pp. 1–2.
[72] B. Kuyken *et al.*, "On-chip parametric amplification with 26.5 dB gain at telecommunication wavelengths using CMOS-compatible hydrogenated amorphous silicon waveguides," *Opt. Lett.*, vol. 36, no. 4, pp. 552–554, Feb. 2011.
[73] J. E. Sharping *et al.*, "Generation of correlated photons in nanoscale silicon waveguides," *Opt. Express*, vol. 14, no. 25, pp. 12388–12393, 2006.
[74] K. Harada *et al.*, "Generation of high-purity entangled photon pairs using silicon wire waveguide," *Opt. Express*, vol. 16, no. 25, pp. 20368–20373, 2008.
[75] S. Clemmen, K. P. Huy, W. Bogaerts, R. G. Baets, P. Emplit, and S. Massar, "Continuous wave photon pair generation in silicon-on-insulator waveguides and ring resonators," *Opt. Express*, vol. 17, no. 19, pp. 16558–16570, 2009.
[76] K. I. Harada *et al.*, "Frequency and polarization characteristics of correlated photon-pair generation using a silicon wire waveguide," *IEEE J. Sel. Topics Quantum Electron.*, vol. 16, no. 1, pp. 325–331, Jan. 2010.
[77] K. Wang *et al.*, "Multichannel photon-pair generation using hydrogenated amorphous silicon waveguides," *Opt. Lett.*, vol. 39, no. 4, pp. 914–917, 2014.
[78] E. Hemsley, D. Bonneau, J. Pelc, R. Beausoleil, J. L. O'Brien, and M. G. Thompson, "Photon pair generation in hydrogenated amorphous silicon microring resonators," *Sci. Rep.*, vol. 6, p. 38908, 2016.
[79] M. Savanier, R. Kumar, and S. Mookherjea, "Photon pair generation from compact silicon microring resonators using microwatt-level pump powers," *Opt. Express*, vol. 24, no. 4, pp. 3313–3328, 2016.
[80] S. Ramelow *et al.* (2015). "Silicon-nitride platform for narrowband entangled photon generation." [Online]. Available: https://arxiv.org/abs/1508.04358
[81] X. Zhang, Y. Zhang, C. Xiong, and B. J. Eggleton, "Correlated photon pair generation in low-loss double-stripe silicon nitride waveguides," *J. Opt.*, vol. 18, p. 074016, 2016.
[82] J. A. Jaramillo-Villegas *et al.*, "Comb-like frequency-bin entangled photon pair generation in silicon nitride microring resonators," in *Proc. Front. Opt. Sci.*, 2016, Paper FW5F.5.
[83] K.-Y. Wang, M. A. Foster, and A. C. Foster, "Wavelength-agile near-IR optical parametric oscillator using a deposited silicon waveguide," *Opt. Express*, vol. 23, no. 12, pp. 15431–15439, 2015.
[84] A. C. Turner-Foster, M. A. Foster, R. Salem, A. L. Gaeta, and M. Lipson, "Frequency conversion over two-thirds of an octave in silicon nanowaveguides," *Opt. Express*, vol. 18, no. 3, pp. 1904–1908, 2010.
[85] K. Saha, Y. Okawachi, O. Kuzucu, M. Mernard, M. Lipson, and A. L. Gaeta, "Chip-scale broadband optical isolation via Bragg scattering four-wave mixing," in *Proc. Conf. Laser Electro-Opt. (CLEO)*, 2013, Paper QF1D.2.
[86] K. Li, H.-F. Ting, M. A. Foster, and A. C. Foster, "High-speed all-optical NAND/AND logic gates using four-wave mixing Bragg scattering," *Opt. Lett.*, vol. 41, no. 14, pp. 3320–3323, 2016.
[87] C. J. Mckinstrie, J. D. Harvey, S. Radic, and M. G. Raymer, "Translation of quantum states by four-wave mixing in fibers," *Opt. Express*, vol. 13, no. 22, pp. 9131–9142, 2005.
[88] A. H. Gnauck, R. M. Jopson, C. J. McKinstrie, J. C. Centanni, and S. Radic, "Demonstration of low-noise frequency conversion by Bragg scattering in a fiber," *Opt. Express*, vol. 14, no. 20, pp. 8989–8994, 2006.
[89] I. Agha, S. Ates, M. Davanço, and K. Srinivasan, "A chip-scale, telecommunications-band frequency conversion interface for quantum emitters," *Opt. Express*, vol. 21, no. 18, pp. 21628–21638, 2013.
[90] Q. Li, M. Davanco, and K. Srinivasan, "Efficient and low-noise single-photon-level frequency conversion interfaces using silicon nanophotonics," *Nature Photon.*, vol. 10, pp. 406–415, 2016.
[91] Y. Zhao, D. Lombardo, J. Mathews, and I. Agha, "Low control-power wavelength conversion on a silicon chip," *Opt. Lett.*, vol. 41, no. 15, pp. 3651–3654, 2016.
[92] B. G. Lee *et al.*, "Demonstration of broadband wavelength conversion at 40 Gb/s in silicon waveguides," *IEEE Photon. Technol. Lett.*, vol. 21, no. 3, pp. 182–184, Feb. 1, 2009.
[93] L. Xu *et al.*, "Simultaneous wavelength conversion of ASK and DPSK signals based on four-wave-mixing in dispersion engineered silicon waveguides," *Opt. Express*, vol. 19, no. 13, pp. 12172–12179, 2011.
[94] K.-Y. Wang, K. G. Petrillo, M. A. Foster, and A. C. Foster, "Ultralow-power all-optical processing of high-speed data signals in deposited silicon waveguides," *Opt. Express*, vol. 20, no. 22, pp. 24600–24606, Oct. 2012.
[95] F. Li *et al.*, "Error-free all-optical demultiplexing at 160 Gb/s via FWM in a silicon nanowire," *Opt. Express*, vol. 18, no. 4, pp. 3905–3910, 2010.
[96] H. Ji *et al.*, "Optical waveform sampling and error-free demultiplexing of 1.28 Tb/s serial data in a nanoengineered silicon waveguide," *J. Lightw. Technol.*, vol. 29, no. 4, pp. 426–431, Feb. 15, 2011.
[97] Y. Zhang *et al.*, "Multichannel phase-sensitive amplification in a low-loss CMOS-compatible spiral waveguide," *Opt. Lett.*, vol. 42, no. 21, pp. 4391–4394, 2017.
[98] H. Sun, K.-Y. Wang, and A. C. Foster, "Pump-degenerate phase-sensitive amplification in amorphous silicon waveguides," *Opt. Lett.*, vol. 42, no. 18, pp. 3590–3593, 2017.
[99] M. Rochette, L. Fu, V. Ta'eed, D. J. Moss, and B. J. Eggleton, "2R Optical regeneration: An all-optical solution for BER improvement," *IEEE J. Sel. Top. Quantum Electron.*, vol. 12, no. 4, pp. 736–743, Jul./Aug. 2006.
[100] A. Biberman *et al.*, "Wavelength multicasting in silicon photonic nanowires," *Opt. Express*, vol. 18, no. 17, pp. 18047–18055, 2010.
[101] M. Pu *et al.*, "One-to-six WDM multicasting of DPSK signals based on dual-pump four-wave mixing in a silicon waveguide," *Opt. Express*, vol. 19, no. 24, pp. 24448–24453, 2011.
[102] H.-F. Ting *et al.*, "Wavelength multicasting through four-wave mixing with an optical comb source," *Opt. Express*, vol. 25, no. 8, pp. 9276–9284, 2017.
[103] Y. Dai *et al.*, "1 μs tunable delay using parametric mixing and optical phase conjugation in Si waveguides," *Opt. Express*, vol. 17, no. 9, pp. 7004–7010, 2009.
[104] Y. Okawachi *et al.*, "Large tunable delays using parametric mixing and phase conjugation in Si nanowaveguides," *Opt. Express*, vol. 16, no. 14, pp. 10349–10357, 2008.
[105] R. Salem, M. A. Foster, A. C. Turner, D. F. Geraghty, M. Lipson, and A. L. Gaeta, "Signal regeneration using low-power four-wave mixing on silicon chip," *Nature Photon.*, vol. 2, no. 1, pp. 35–38, Jan. 2008.
[106] F. Li *et al.*, "All-optical XOR logic gate for 40 Gb/s DPSK signals via FWM in a silicon nanowire," *Opt. Express*, vol. 19, no. 21, pp. 20364–20371, Oct. 2011.
[107] Y. Xie, Y. Gao, S. Gao, X. Mou, and S. He, "All-optical multiple-channel logic XOR gate for NRZ-DPSK signals based on nondegenerate four-wave mixing in a silicon waveguide," *Opt. Lett.*, vol. 36, no. 21, pp. 4260–4262, 2011.

[108] J. Hou, L. Chen, W. Dong, and X. Zhang, "40 Gb/s reconfigurable optical logic gates based on FWM in silicon waveguide," *Opt. Express*, vol. 24, no. 3, pp. 2701–2711, 2016.
[109] S. Gao, X. Wang, Y. Xie, P. Hu, and Q. Yan, "Reconfigurable dual-channel all-optical logic gate in a silicon waveguide using polarization encoding," *Opt. Lett.*, vol. 40, no. 7, pp. 1448–1451, 2015.
[110] K. Li and A. C. Foster, "1.25-Gb/s all-optical NAND/AND logic gates in a hydrogenated amorphous silicon waveguide," in *Proc. Conf. Laser Electrp-Opt.*, 2017, Paper SM1M.3.
[111] U. Willer, M. Saraji, A. Khorsandi, P. Geiser, and W. Schade, "Near- and mid-infrared laser monitoring of industrial processes, environment and security applications," *Opt. Lasers Eng.*, vol. 44, no. 7, pp. 699–710, 2006.
[112] D. S. Moore, "Instrumentation for trace detection of high explosives," *Rev. Sci. Instrum.*, vol. 75, no. 8, pp. 2499–2512, 2004.
[113] M. Yu, Y. Okawachi, A. G. Griffith, M. Lipson, and A. L. Gaeta, "Modelocked mid-infrared frequency combs in a silicon microresonator," *Optica*, vol. 3, no. 8, pp. 854–860, 2016.
[114] X. Liu, B. Kuyken, G. Roelkens, R. Baets, R. M. Osgood, Jr., and W. M. J. Green, "Bridging the mid-infrared-to-telecom gap with silicon nanophotonic spectral translation," *Nature Photon.*, vol. 6, pp. 667–671, Sep. 2012.
[115] X. Liu, R. M. Osgood, Jr., Y. A. Vlasov, and W. M. J. Green, "Mid-infrared optical parametric amplifier using silicon nanophotonic waveguides," *Nature Photon.*, vol. 4, pp. 557–560, May 2010.
[116] G. Z. Mashanovich *et al.*, "Silicon photonic waveguides and devices for near- and mid-IR applications," *IEEE J. Sel. Topics Quantum Electron.*, vol. 21, no. 4, Jul./Aug. 2015, Art. no. 8200112.
[117] T. Udem, R. Holzwarth, and T. W. Hänsch, "Optical frequency metrology," *Nature*, vol. 416, no. 6877, pp. 233–237, 2002.
[118] S. B. Papp *et al.*, "Microresonator frequency comb optical clock," *Optica*, vol. 1, no. 1, pp. 10–14, 2014.
[119] R. Holzwarth *et al.*, "Optical frequency synthesizer for precision spectroscopy," *Phys. Rev. Lett.*, vol. 85, no. 11, pp. 2264–2267, 2000.
[120] D. T. Spencer, T. Drake, and S. B. Papp, "An optical-frequency synthesizer using integrated photonics," *Nature*, vol. 557, pp. 81–85, Apr. 2018.
[121] M. Yu, Y. Okawachi, A. G. Grif, N. Picqué, M. Lipson, and A. L. Gaeta, "Silicon-chip-based mid-infrared dual-comb spectroscopy," *Nature Commun.*, vol. 9, pp. 1–6, May 2018.
[122] X. Xu *et al.*, "Advanced RF and microwave functions based on an integrated optical frequency comb source," *Opt. Express*, vol. 26, no. 3, pp. 2569–2583, 2018.
[123] J. Pfeifle *et al.*, "Coherent terabit communications with microresonator Kerr frequency combs," *Nature Photon.*, vol. 8, no. 5, pp. 375–380, 2014.
[124] C. Reimer *et al.*, "Integrated frequency comb source of heralded single photons," *Opt. Express*, vol. 22, no. 6, pp. 6535–6546, 2014.
[125] C. Reimer *et al.*, "Generation of multiphoton entangled quantum states by means of integrated frequency combs," *Science*, vol. 351, no. 6278, pp. 1176–1180, 2016.
[126] A. Dutt *et al.*, "Dual-comb Spectroscopy using On-chip Mode-locked Frequency Combs," in *Proc. Conf. Laser Electro-Opt.*, 2017, Paper STh3L.2.
[127] Y. Okawachi, K. Saha, J. S. Levy, Y. H. Wen, M. Lipson, and A. L. Gaeta, "Octave-spanning frequency comb generation in a silicon nitride chip," *Opt. Lett.*, vol. 36, no. 17, pp. 3398–3400, 2011.
[128] F. Ferdous *et al.*, "Spectral line-by-line pulse shaping of on-chip microresonator frequency combs," *Nature Photon.*, vol. 5, pp. 770–776, Oct. 2011.
[129] Y. Liu *et al.*, "Investigation of mode coupling in normal-dispersion silicon nitride microresonators for Kerr frequency comb generation," *Optica*, vol. 1, no. 3, pp. 137–144, 2014.
[130] Q. Li *et al.*, "Stably accessing octave-spanning microresonator frequency combs in the soliton regime," *Optica*, vol. 4, no. 2, pp. 193–203, 2017.
[131] Y. K. Chembo, "Kerr optical frequency combs: Theory, applications and perspectives," *Nanophotonics*, vol. 5, no. 2, pp. 214–230, 2016.
[132] S. Sicari, A. Rizzardi, L. A. Grieco, and A. Coen-Porisini, "Security, privacy and trust in Internet of Things: The road ahead," *Comput. Netw.*, vol. 76, pp. 146–164, Jan. 2015.
[133] D. Grassani *et al.*, "Micrometer-scale integrated silicon source of time-energy entangled photons," *Optica*, vol. 2, no. 2, pp. 88–94, 2015.
[134] C. Xiong *et al.*, "Active temporal multiplexing of indistinguishable heralded single photons," *Nature Commun.*, vol. 7, pp. 1–6, Mar. 2016.
[135] C. Xiong, B. Bell, and B. J. Eggleton, "CMOS-compatible photonic devices for single-photon generation," *Nanophotonics*, vol. 5, no. 3, pp. 427–439, 2016.
[136] P. Sibson, J. E. Kennard, S. Stanisic, C. Erven, J. L. O'Brien, and M. G. Thompson, "Integrated silicon photonics for high-speed quantum key distribution," *Optica*, vol. 4, no. 2, pp. 172–177, 2017.
[137] B. C. Grubel *et al.*, "Silicon photonic physical unclonable function," *Opt. Express*, vol. 25, no. 11, pp. 12710–12721, 2017.
[138] B. C. Grubel, B. T. Bosworth, M. R. Kossey, A. B. Cooper, M. A. Foster, and A. C. Foster, "Secure communications using nonlinear silicon photonic keys," *Opt. Express*, vol. 26, no. 4, pp. 4710–4722, 2018.
[139] C. J. Krückel, A. Fülöp, T. Klintberg, J. Bengtsson, P. A. Andrekson, and V. Torres-Company, "Linear and nonlinear characterization of low-stress high-confinement silicon-rich nitride waveguides," *Opt. Express*, vol. 23, no. 20, pp. 25827–25837, 2015.
[140] M. R. Dizaji, C. J. Krückel, A. Fülöp, P. A. Andrekson, V. Torres-Company, and L. R. Chen, "Silicon-rich nitride waveguides for ultra-broadband nonlinear signal processing," *Opt. Express*, vol. 25, no. 11, pp. 12100–12108, 2017.
[141] C. Lacava *et al.*, "Si-rich silicon nitride for nonlinear signal processing applications," *Sci. Rep.*, vol. 7, Feb. 2017, Art. no. 22.
[142] N. K. Hon, R. Soref, and B. Jalali, "The third-order nonlinear optical coefficients of Si, Ge, and Si1-xGex in the midwave and longwave infrared," *J. Appl. Phys.*, vol. 110, no. 1, p. 011301, 2011.
[143] L. Carletti *et al.*, "Nonlinear optical response of low loss silicon germanium waveguides in the mid-infrared," *Opt. Express*, vol. 23, no. 7, pp. 8261–8271, 2015.
[144] M. A. Ettabib *et al.*, "All-optical phase regeneration with record PSA extinction ratio in a low-birefringence silicon germanium waveguide," *J. Lightw. Technol.*, vol. 34, no. 17, pp. 3993–3998, Sep. 2016.
[145] D. Lyu, Q. Jin, and S. Gao, "Design of mid-infrared nonlinear silicon-germanium waveguides for broadband/discrete-band wavelength conversion," *J. Opt. Soc. Amer. B, Opt. Phys.*, vol. 35, no. 4, pp. 741–751, 2018.
[146] S. Serna *et al.*, "Nonlinear properties of Ge-rich Si1-xGex materials with different Ge concentrations," *Sci. Rep.*, vol. 7, no. 1, pp. 1–11, 2017.
[147] A. H. Hosseinnia, A. H. Atabaki, A. A. Eftekhar, and A. Adibi, "High-quality silicon on silicon nitride integrated optical platform with an octave-spanning adiabatic interlayer coupler," *Opt. Express*, vol. 23, no. 23, pp. 30297–30307, 2015.
[148] M. Kossey, K. Li, H. Sun, and A. C. Foster, "Four-wave mixing in a multi-layer SiNx/a-Si:H photonic chip," in *Proc. Conf. Laser Electro-Opt.*, 2018, Paper STh3I.5.

ABOUT THE AUTHORS

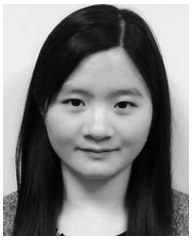

Kangmei Li (Student Member, IEEE) received the B.S. degree in physics from Peking University, Beijing, China, in 2012 and the M.S. degree in electrical and computer engineering from Johns Hopkins University, Baltimore, MD, USA, in 2014, where she is currently working toward the Ph.D. degree at the Integrated Photonics Laboratory.

Her research interests include the development of ultrawide bandwidth integrated photonic devices and high-speed optical communication systems.

Amy C. Foster (Member, IEEE) was born in Rochester, NY, USA. She received the B.S. degree in electrical engineering from the University at Buffalo, Buffalo, NY, USA, in 2003 and the M.S. and Ph.D. degrees in electrical and computer engineering from Cornell University, Ithaca, NY, USA, in 2007 and 2009, respectively.

She is currently an Associate Professor at the Electrical and Computer Engineering Department, Johns Hopkins University, Baltimore, MD, USA. She has over 40 journal and over 70 conference proceedings publications in the area of silicon photonics. Her research has primarily focused on nanoscale-control of silicon-based integrated photonic waveguides for optimizing interactions such as nonlinear parametric processes.

Prof. Foster has been a recipient of the DARPA Young Faculty Award, as well as the Johns Hopkins University Catalyst Award. She is a member of the Optical Society of America (OSA) and the American Physical Society (APS), and is serving on the IEEE Photonics Conference Optical Interconnects committee. She previously served as the Co-Director of the 49th Annual IEEE Conference on Information Sciences and Systems (2015). She is an Associate Editor of the OSA journal *Optics Express*.